

Learning Sparse Visual Representations with Leaky Capped Norm Regularizers

Jianqiao Wangni*
Tsinghua University
Beijing, China
zjnqha@gmail.com

Dahua Lin
The Chinese University of Hong Kong
Hong Kong, China
dhlin@ie.cuhk.edu.hk

Abstract

Sparsity inducing regularization is an important part for learning over-complete visual representations. Despite the popularity of ℓ_1 regularization, in this paper, we investigate the usage of non-convex regularizations in this problem. Our contribution consists of three parts. First, we propose the leaky capped norm regularization (LCNR), which allows model weights below a certain threshold to be regularized more strongly as opposed to those above, therefore imposes strong sparsity and only introduces controllable estimation bias. We propose a majorization-minimization algorithm to optimize the joint objective function. Second, our study over monocular 3D shape recovery and neural networks with LCNR outperforms ℓ_1 and other non-convex regularizations, achieving state-of-the-art performance and faster convergence. Third, we prove a theoretical global convergence speed on the 3D recovery problem. To the best of our knowledge, this is the first convergence analysis of the 3D recovery problem.

Introduction

The sparse models have been widely applied in machine learning and computer vision tasks. To encourage sparsity, the ℓ_1 norm is widely adopted as a regularizer, which can produce reasonable results in various cases. For an example, to analyse the 3D shape of an object, from a monocular 2D camera, one can build a dictionary of 3D shape bases from datasets, and inference the sparse combination weights of the bases (Zhou et al. 2016). Yet, a number of studies suggested that it is not always the optimal choice, *non-convex* regularizers can often lead to better balance between sparsity and accuracy in practice. Particularly, a number of non-convex regularizers have been explored in previous work, such as ℓ_p norm (Frank et al. 1993), MCP (Zhang 2010a), SCAD (Fan and Li 2011), Logarithm (Friedman 2012), and capped norm (Zhang 2010b)(Zhang and others 2013). However, the studied models are mostly restricted to be convex ones, therefore lack suitability to larger application scope. This is reasonable since, first, the convex problem with non-convex regularizers are already difficult to analyse, the global optima can only be obtained with additional statistical assumptions. The non-convex problem, even without

*This work was done when the first author was a visiting research assistant at CUHK.

regularizers, is much more difficult to optimize, the solver for non-convex will converges much slower comparing to when it applies to convex ones.

In this work, we will concentrate on the learning better sparse models, with considerations on the running time limitation, which commonly exists, especially in testing stage. For an example, the aforementioned 3D shape recovery models have achieved good enough accuracy, but they converge too slow for real-time applications. Although directly enlarging the ℓ_1 regularizer will force more small weights to be zeros within limited time, but this will certainly compromise the accuracy since the larger and effective weights are also penalized strongly. In this work, we aim to move beyond the limitations of existing literatures and develop a novel regularizer that can achieve high sparsity and high accuracy in learning sparse representations (like other successful applications based on non-convex regularizers). The key to achieve this goal is to force more smaller weights to zeros by a stronger regularization, but not so far as to leading larger weights deviating from the ground truth. Following this idea, we propose a novel non-convex regularizer, called *Leaky Capped Norm*, which is a generalization of the capped norms, but enjoys nice mathematical properties and demonstrates higher performance in experiments. We also derive a doubly majorization-minimization algorithm, which is suitable for both convex and nonconvex loss functions. We also take the 3D shape recovery problem for detailed analysis. By relaxing the objective to a convex one, we can apply an ADMM solver and get a theoretical global convergence. We also conducted experiments on sparse neural networks to show the efficiency in compressing kernel weights.

Leaky Capped ℓ_1 Norm

A standard sparse model consists of a loss function L (which we assume to be differentiable but possibly nonconvex) and a regularization part H on the weights c

$$\min_c \frac{1}{N} \sum_n L(x_n, c) + H(c). \quad (1)$$

where $\{x_n\}$ are data points. A popular choice for H is the ℓ_1 norm, due to its convenience for optimization and that it is good surrogate for ℓ_0 norm. There are also some literatures suggesting that the ℓ_1 norm is in many case inferior

to non-convex norms for inducing sparsity. To motivate our new regularizer, we begin with a discussion on the representative capped ℓ_1 norm (Zhang 2010b):

$$H(c) = \alpha \sum_i \min(|c_i|, \tau), \quad \text{where } \alpha, \tau > 0. \quad (2)$$

As shown in Figure 1, this formulation only regularizes those weights that are below a certain threshold τ . For those beyond this value, they can grow arbitrarily without experiencing penalties. It is noteworthy that it is a generalization of ℓ_1 norm. Particularly, it becomes ℓ_1 as $\tau \rightarrow \infty$. Generally, with a finite τ , it approximates ℓ_0 better than ℓ_1 , and therefore leads to higher sparsity in some real-world applications. The key feature of capped norm is the lack of penalty

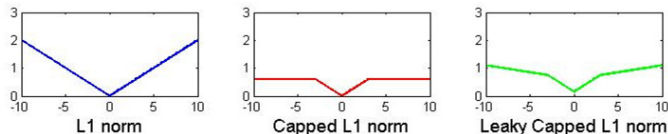


Figure 1: Geometric view of three kinds of norms.

for weights whose magnitudes are greater than τ , this feature, however, may become a drawback under some circumstances. For examples, in our empirical study on 3D shape recovery, which is introduced later, the capped norm leads to unstable optimization procedures and substantially worse solutions, by the multi-stage algorithm introduced later. Another difficulty shared by both ℓ_1 and capped ℓ_1 norms is the parameters selection – it is often very tricky to find a good value of τ and α that well balances between accuracy and sparsity. From an optimization perspective, the two parameters are both critical to the most common proximal operator, as

$$\arg \min_x \frac{1}{2} \|x - c\|^2 + H(x) = \text{sign}(c) \max(|c| - \mathbb{I}(c < \tau)\alpha, 0),$$

where $\mathbb{I}(\cdot)$ is the indicator function that equals to one for truth and zero for false. As implied by theoretical analysis and shown in our experiments, larger values of α and τ would yield sparser solutions, but at the same time damage the larger weights and consequently compromise the accuracy. With the analysis above in mind, we propose the *Leaky Capped ℓ_1 Norm Regularizer (LCNR)* as an improved variant:

$$H(c) = \alpha \sum_i \min(|c_i|, \tau) + \beta \sum_i \max(|c_i|, \tau), \quad (3)$$

where $0 < \beta < \alpha$. As shown in Figure 1, the function of LCNR is piecewise linear and thus is differentiable (except at a few points). The key difference between the proposed formulation and the standard ℓ_1 norm and the capped norm is that large weights (*i.e.* those greater than τ) are still penalized *positively* but *less heavily*. To be more specific, this generalizes the capped ℓ_1 norm, with an additional coefficient β to control how much those large weights are regularized. In particular, when $\beta = 0$, it reduces to the regular capped norm.

A representative optimization algorithm for solving convex problems with nonconvex regularizer is the multi-stage algorithm (Zhang 2010b), it is guaranteed to converge since it is essentially a special case of the majorization-minimization (MM) algorithm (Hunter and Lange 2004). To be more specific, at the $(l + 1)$ -th stage, the surrogate objective is

$$H^{l+1}(c) = |c^T| \cdot \lambda^l, \quad \text{where } \lambda_i^l = \alpha \mathbb{I}(|c_i^l| \leq \tau) + \beta \mathbb{I}(|c_i^l| > \tau),$$

where c^l is the optimal c at the l -th stage, but the surrogate loss remains the same as original one. We set the initialization parameter $\lambda_i^0 = \beta$, so as to begin with a light regularization for all weights. Based on the algorithm, one can see that the parameter selection is simpler - one can first search β for accuracy and then α for sparsity.

Monocular 3D Shape Recovery

Now we proceed to demonstrating the usage of the proposed regularizer and algorithms for solving a computer vision problem, the 3D shape analysis of visual objects. Driven by the demands arising from real-world applications, 3D shape recovery from 2D images has received increasing attention from the computer vision community in recent years. A key challenge of this task lies in the fact that different 3D shapes can be projected to the same 2D image, resulting in an ill-posed problem. A commonly adopted approach is to restrict the recovered 3D shape to be a linear combination of a set predefined shape bases. A representative model in early ages along this line is the Active Shape Model (ASM)(Cootes et al. 1995), which relies on a dense combination for shape representation. Later advances, like (Hejrati and Ramanan 2012)(Zia et al. 2013)(Wang et al. 2014)(Xiang and Savarese 2012)(Ramakrishna, Kanade, and Sheikh 2012)(Lin et al. 2014)however, shows that sparse representation is more effective in real-world applications, often demonstrating stronger generalization performance and higher robustness against adverse conditions.

The 3D shape, *i.e.* the 3D locations of p landmarks are stacked as $S \in \mathbb{R}^{3 \times p}$, and its corresponding 2D shape is $Y \in \mathbb{R}^{2 \times p}$. We denote the projection matrix as Π . The Active Shape Models (ASM) (Cootes et al. 1995) proposed training a group of shape bases $\{B_i\}_{i=1}^D$ from data by methods like principal component analysis, denoting $\mathcal{D} = \{1, \dots, D\}$ as a set of subscripts and c as weights of each basis. The 3D-2D shape relation is characterized as

$$S = \sum_{i \in \mathcal{D}} c_i B_i, \quad Y = \Pi S,$$

$$\text{where } \Pi = \begin{pmatrix} \omega & 0 & 0 \\ 0 & \omega & 0 \end{pmatrix}, c \in \mathbb{R}^D, B_i \in \mathbb{R}^{3 \times p} \quad (4)$$

here ω is a parameter depending on physical factors like focal length and view depth. In the test phase, the 2D shape Y is annotated by regular visual detectors, since the shape bases B are most likely predefined in a different camera setting other than the test setting, the unknown factors including combination weights c , a relative rotation parameter R and a translation parameter T should all be considered in the

projection model,

$$Y = \Pi(R \sum_{i \in \mathcal{D}} c_i B_i + T), \text{ where } R \in SO(3), T \in \mathbb{R}^3 \quad (5)$$

where $I_3 \in \mathbb{R}^{3 \times 3}$ is an identity matrix and $SO(3) = \{R \in \mathbb{R}^{3 \times 3} \mid R^T R = I_3, \det(R) = 1\}$. In addition, (Zhou et al. 2016) proposed distributing individual rotation matrix $R_i \in \mathbb{R}^{3 \times 3}$ to each basis, then the 3D and 2D shapes are represented as $= \sum_{i \in \mathcal{D}} c_i R_i B_i$. They substitute the bilinear term composed of Π and R by uniform variables $\{M_i \in \mathbb{R}^{2 \times 3}\}_{i \in \mathcal{D}}$, that $M_i = c_i \Pi R_i$ which implicitly take rotation and projection factors into account. Denoting M as a 3 dimensional tensor stacking $\{M_i\}_{i=1}^D$, we rewrite the objective as

$$\min_{R_i \in \Omega(c_i), c} F(M, c) = \frac{1}{2} \|Y - \sum_{i \in \mathcal{D}} M_i B_i\|_F^2 + H(c), \quad (6)$$

$$\text{where } \Omega(c_i) = \{M_i \in \mathbb{R}^{2 \times 3} \mid M_i^T M_i = c_i^2 I_2\},$$

and $H(c)$ is the regularization and $I_2 \in \mathbb{R}^{2 \times 2}$ is an identity matrix. In our model of 3D shape recovery, we adopt the linear formulation as Eq.(6) since it is the best baseline up until now and has some attractive properties. Our objective function is same with Eq.(6), $H(c)$ is set to be LCNR as Eq.(3). The objective with a stage-wise surrogate regularizer is

$$F^{l+1}(M, c) = \frac{1}{2} \|Y - \sum_{i \in \mathcal{D}} M_i B_i\|_F^2 + \sum_{i \in \mathcal{D}} \lambda_i^l |c_i|, \quad (7)$$

in the $(l+1)$ -th stage, where $M_i \in \Omega(c_i)$. In this optimizer, the regularization part of $F(R, c)$ is convex in each stage, however, the surrogate function is still non-convex since there is an orthogonality constraint on each M_i . To build the upper bounding function, we make a convex relaxation on the constraints. As the spectral-norm ball $\text{conv}(\Omega(c_i)) = \{X \in \mathbb{R}^{2 \times 3} \mid \|X\|_2 \leq c_i\}$, is the tightest convex hull of the Stiefel manifold $\Omega(c_i)$ (Zhou et al. 2016) [(Journée et al. 2010), Section 3.4], where $\|\cdot\|_2$ represents the spectral norm, which is its largest singular value. Finally, by relaxing the domain Ω to $\text{conv}(\Omega)$, and the recalibration rule of λ_i is transferred to $\lambda_i^l = \alpha \mathbb{I}(\|\hat{M}_i^l\|_2 \leq \tau) + \beta \mathbb{I}(\|\hat{M}_i^l\|_2 > \tau)$, where \hat{M}_i^l is the optimal M_i in the l -th stage.

Since the function is convexified, We employ the alternate direction method of multiplier (ADMM) (Boyd et al. 2011)(Zhou et al. 2016) algorithm to attain high-precision solutions. We introduce a tensor V as a copy of M , U as a dual tensor variable and μ as a stepsize parameter, then rewrite Eq.(7) in its augmented Lagrangian formulation

$$F_\mu^{l+1}(M, V, U) = \frac{1}{2} \|Y - \sum_{i \in \mathcal{D}} V_i B_i\|_F^2 + \sum_{i \in \mathcal{D}} \lambda_i^l \|M_i\|_2 + \sum_{i \in \mathcal{D}} U_i^T (M_i - V_i) + \frac{\mu}{2} \sum_{i \in \mathcal{D}} \|M_i - V_i\|^2 \quad (8)$$

Then the ADMM procedure is applied to solve the subproblem. After the convergence, the multi-stage solver will update the surrogate functions. We denote the inner-iteration

superscript as t . Then M^{t+1} is update based on the proximal operator on spectral norms [(Parikh, Boyd, and others 2014), Section 6.7.2],

$$\text{prox}_{\lambda}(V_i^t) = P \text{diag}[\sigma - \lambda_i^t \mathcal{P}_1(\sigma/\lambda_i^t)] Q^T, \quad (9)$$

where $V_i^t = V_i^t - U_i^t/\mu$ and $\lambda_i^t = \lambda_i^t/\mu$. Denoting the solution as $\text{prox}_{\lambda_i^t}(V_i^t)$, $V_i^t = P \text{diag}(\sigma) Q^T$ is the singular value decomposition of V_i^t , and $\mathcal{P}_1(\cdot)$ is the Euclidean projection onto the ℓ_1 norm ball. The update on V and U have closed form solutions,

$$V_i^{t+1} = (Y B_i^T + \mu M_i^{t+1} + U_i^{t+1})(B_i B_i^T + \mu I_3)^{-1}, \quad (10)$$

$$U_i^{t+1} = U_i^t + \mu(M_i^t - V_i^t). \quad (11)$$

The convergence property of this algorithm is well studied in (Boyd et al. 2011), additionally, we adopt an adaptive policy for stepsize μ as suggested by [(Boyd et al. 2011), Section 3].

Theoretical Analysis

Generally speaking, the convergence of optimization over non-convex function is typical hard to prove without a decreasing step size. When combined with nonconvex regularizers, even convex problems need highly specialized proofs, for each problem. One may see the hardness of by referring to literatures, on the theoretical analysis of capped norm in different applications, *e.g.*, multi-task feature learning (Gong, Ye, and Zhang 2012)(Tang, Nie, and Jain 2016), matrix completion (Gao et al. 2015) and (Jiang, Nie, and Huang 2015)(Sun, Xiang, and Ye 2013)(Han and Zhang 2016)(Zhang 2010b)(Zhang and others 2013). The proof is harder for our problem since the loss function is already non-convex. In this section, we theoretically prove that with a high probability, the recovery error of our multi-stage algorithm decreases at nearly exponential speed against stages. We assume that the ground truth of the 2D shape $\bar{Y} \in \mathbb{R}^{2 \times p}$ is expressed as a projection of the combined deformation of 3D shape bases, as $\bar{Y} = \sum_{i \in \mathcal{D}} \bar{M}_i B_i$, where \bar{M}_i is the ground truth of deformation matrix M_i , for $0 \leq i \leq D$. The observation model is $Y = \bar{Y} + \delta$, where $\delta \in \mathbb{R}^{2 \times p}$ is a Gaussian noise, *i.e.* $\delta_{jk} \sim \mathcal{N}(0, \sigma^2)$. For notational simplicity, we also set $\gamma = \alpha + \beta$.

Assumption 1 For any matrix $M_i \in \mathbb{R}^{n \times m}$, we assume that there exist a constant κ_i that

$$\kappa_i = \min_{M_i \in \mathcal{R}(s)} \|Z - M_i B_i\|_F / \|M_i\|_* > 0, \quad (12)$$

where the restricted set $\mathcal{R}(s)$ is defined as $\mathcal{R}(s) = \{X \in \mathbb{R}^{n \times m} \mid \text{rank}(X) \leq s\}$.

Remark 1 This is the widely used eigenvalue assumption which can be found in (Lounici et al. 2009).

Theorem 2 Following the common setting of sparse dictionary learning, we assume that each basis B_i are normalized by row ℓ_2 norm that $\sum_k B_{irk}^2 = \phi$ for all $i \in \mathcal{D}, 1 \leq r \leq 3$, where ϕ is an constant. For the optimal matrix $\hat{M}_i \in \mathbb{R}^{2 \times 3}$ in any stage, if we set α, β as $(\alpha + \beta) \geq \phi\sqrt{3} + e/2$, then it

holds

$$\frac{1}{2}\|\bar{Y} - \sum_{i \in \mathcal{D}} \hat{M}_i B_i\|_F^2 \leq \frac{1}{2}\|\bar{Y} - \sum_{i \in \mathcal{D}} M_i B_i\|_F^2 + \sum_{i \in \mathcal{D}} (4\gamma + \lambda_i^l) \|M_i - \hat{M}_i\|_2, \quad (13)$$

with the probability of at least $1 - 2D \exp(-\frac{1}{2}(e - 3 \ln(1 + e/3)))$, where e is a positive scalar.

Proof. Recalling that $Y = \bar{Y} + \delta$ and the property of optimal point \hat{M}_i , then we have

$$\frac{1}{2}\|\bar{Y} - \sum_{i \in \mathcal{D}} \hat{M}_i B_i\|_F^2 \leq \frac{1}{2}\|\bar{Y} - \sum_{i \in \mathcal{D}} M_i B_i\|_F^2 \quad (14)$$

$$+ \sum_{i \in \mathcal{D}} \lambda_i^l \|M_i - \hat{M}_i\|_2 + \sum_{i \in \mathcal{D}} \text{tr}[(M_i - \hat{M}_i) B_i \delta^T], \quad (15)$$

where we use the triangular inequality of spectral norm

$$\|M_i\|_2 - \|\hat{M}_i\|_2 \leq \|M_i - \hat{M}_i\|_2. \quad (16)$$

We first establish the upper bound of $\text{tr}[(\hat{M}_i - M_i) B_i \delta^T]$. We denote a set of random events $\{\mathcal{A}_{ij}\}$ and define a set of random variables $\{v_{ijr}\}$ as

$$\mathcal{A}_{ij} = \{\|B_i^T \delta_j\|_2 \leq \phi\gamma\}, \quad v_{ijr} = \frac{1}{\phi} \sum_{k=1}^p B_{irk} \delta_{jk}, \quad (17)$$

where B_{irk} is the element in the r -th row and k -th column of B_i . Since B_i is normalized, v_{ijr} are i.i.d. Gaussian variables following $\mathcal{N}(0, 1)$. Then we can verify that $\sum_{r=1}^3 v_{ijr}^2$ is a chi-squared random variable with $d = 3$ degree of freedom. By choosing λ according to Theorem 2, we have

$$\begin{aligned} Pr(\frac{1}{2}\|B_i \delta_j^T\|_2 > \gamma) &= Pr(\sum_{r=1}^3 (\sum_{k=1}^p B_{irk} \delta_{jk})^2 > 4\gamma^2) \\ &\leq Pr(\sum_{r=1}^3 v_{ijr}^2 > 3 + e) \leq \exp(-\frac{1}{2}\theta(e)), \end{aligned} \quad (18)$$

where $\theta(e) = e - 3 \ln(1 + e/3)$ and the second inequality is due to the chi-squared distribution (Chen, Zhou, and Ye 2011). Denoting $\mathcal{A} = \bigcap_{i=1}^D \bigcap_{j=1}^2 \mathcal{A}_{ij}$, we also denote \mathcal{A}^c as its complementary set and $|\mathcal{A}|$ as its cardinality, then

$$Pr(\mathcal{A}) = 1 - \bigcup_{i=1}^D \bigcup_{j=1}^2 \mathcal{A}_{ij}^c \geq 1 - 2D \exp(-\frac{1}{2}\theta(e)). \quad (19)$$

Denoting M_{ir} as the r -th row of M_i , we can derive an upper bound on $\text{tr}[(\hat{M}_i - M_i) B_i \delta^T]$ under the event \mathcal{A} ,

$$\begin{aligned} \text{tr}[(M_i - \hat{M}_i) B_i \delta^T] &= \sum_{r=1}^2 \sum_{j=1}^2 (M_{ir} - \hat{M}_{ir})^T B_i \delta_j^T \\ &\leq \sum_{r=1}^2 \sum_{j=1}^2 \|M_{ir} - \hat{M}_{ir}\|_2 \|B_i \delta_j^T\|_2 \leq 4\gamma \|M_i - \hat{M}_i\|_2, \end{aligned} \quad (20)$$

where we apply the Cauchy-Schwarz inequality and the relation between Frobenius norm and spectral norm. By substituting this back to Eq.(14), we get the proof.

Theorem 3 Let \hat{M}_i^{l+1} be the optimal solution at the $(l+1)$ -th stage, and \hat{M}_i^l be the one at the l -th stage accordingly. We define $W_i^l = M_i - \hat{M}_i^l$, and a function \mathcal{L} on set $\mathcal{S} \subseteq \mathcal{D}$. If we choose α, β as in Theorem 1 and choose τ as $\tau > (\alpha + \beta)/\kappa^2$, the following inequality stands

$$\mathcal{L}_{l+1}(\mathcal{D}) \leq a^l \mathcal{L}_0(\mathcal{D}) + \frac{b}{1-a}, \quad \text{where } \mathcal{L}_l(\mathcal{S}) = \sqrt{\sum_{i \in \mathcal{S}} \|W_i^l\|_2^2},$$

with probability of at least $1 - 2D \exp(-\frac{1}{2}(e - 3 \ln(1 + e/3)))$, where $a = (\alpha + \beta)/(\kappa^2 \tau)$, and $b = 5(\alpha + \beta)\sqrt{D}/(\kappa^2 \tau)$.

Proof. We apply Theorem 2 in stage $(l+1)$ and substitute M by its ground truth \bar{M} , then get

$$\frac{1}{2}\|\bar{Y} - \sum_{i \in \mathcal{D}} \hat{M}_i^{l+1} B_i\|_F^2 \leq \sum_{i \in \mathcal{D}} (4\gamma + \lambda_i^l) \|W_i^{l+1}\|_2, \quad (21)$$

where we use $\bar{Y} = \sum_{i \in \mathcal{D}} \bar{M}_i B_i$. We define a set $\mathcal{G} = \{i \in \mathcal{D} \mid \|\hat{M}_i^l\|_2 \leq \tau\}$ to separate the weights, and

$$\alpha_i^l = \alpha \mathbb{I}(i \in \mathcal{G}), \quad \beta_i^l = \beta \mathbb{I}(i \in \mathcal{G}^c), \quad (22)$$

then there is $\lambda_i^l = \alpha_i^l + \beta_i^l$. Then we establish a bound by Cauchy-Schwarz inequality,

$$\begin{aligned} \sum_{i \in \mathcal{D}} (\lambda_i^l + 4\gamma) \|W_i^{l+1}\|_2 &= \sum_{i \in \mathcal{D}} (\alpha_i^l + \beta_i^l + 4\gamma) \|W_i^{l+1}\|_2 \\ &\leq (4\gamma\sqrt{D} + \alpha\sqrt{|\mathcal{G}|} + \beta\sqrt{|\mathcal{G}^c|}) \mathcal{L}_{l+1}(\mathcal{D}). \end{aligned} \quad (23)$$

To further bound this term, we first denote that

$$\mathcal{E} = \{i \in \mathcal{D} \mid \|\bar{M}_i\|_2 \neq 0\}, \quad \mathcal{F} = \{i \in \mathcal{D} \mid \|\bar{M}_i\|_2 \leq 2\tau\}, \quad (24)$$

by the rule of set operation and the definition of \mathcal{G} and \mathcal{F} ,

$$|\mathcal{G}| = |\mathcal{G} \cap \mathcal{F}| + |\mathcal{G} \cap \mathcal{F}^c|, \quad \text{where } |\mathcal{G} \cap \mathcal{F}| \leq |\mathcal{F}|, \quad (25)$$

$$\tau^2 |\mathcal{G} \cap \mathcal{F}^c| \leq \sum_{i \in \mathcal{G} \cap \mathcal{F}^c} \|\bar{M}_i - \hat{M}_i^l\|_2^2 \leq \mathcal{L}_i^2(\mathcal{G} \cap \mathcal{F}^c); \quad (26)$$

by the inequality $\|\bar{M}_i - \hat{M}_i^l\|_2 \geq \|\bar{M}_i\|_2 - \|\hat{M}_i^l\|_2 \geq \tau$. Substituting them back to Eq.(23), we get

$$\sum_{i \in \mathcal{D}} \alpha_i^l \|W_i^{l+1}\|_2 \leq \alpha \sqrt{|\mathcal{F}|} + \mathcal{L}_i^2(\mathcal{F}^c)/\tau^2 \mathcal{L}_{l+1}(\mathcal{D}) \quad (27)$$

$$\leq (\alpha \sqrt{|\mathcal{F}|} + \frac{\alpha}{\tau} \mathcal{L}_l(\mathcal{F}^c)) \mathcal{L}_{l+1}(\mathcal{D}), \quad (28)$$

where in the last inequality we use $\sqrt{a^2 + b^2} \leq a + b$ for $a, b \geq 0$. A similar result holds for another part of Eq.(23) as

$$\sum_{i \in \mathcal{D}} \beta_i^l \|W_i^{l+1}\|_2 \leq (\beta \sqrt{|\mathcal{E}|} + \frac{\beta}{\tau} \mathcal{L}_l(\mathcal{E}^c)) \mathcal{L}_{l+1}(\mathcal{D}). \quad (29)$$

Substituting them back to Eq.(21), there is

$$\begin{aligned} \frac{1}{2}\|\bar{Y} - \sum_{i \in \mathcal{D}} \hat{M}_i^{l+1} B_i\|_F^2 &\leq \sum_{i \in \mathcal{D}} (4\gamma + \lambda_i^l) \|W_i^{l+1}\|_2 \\ &\leq \gamma(4\sqrt{D} + \sqrt{\max(|\mathcal{E}|, |\mathcal{F}|)}) + \frac{1}{\tau} \mathcal{L}_l(\mathcal{D}) \mathcal{L}_{l+1}(\mathcal{D}), \end{aligned} \quad (30)$$

Recalling Assumption 1 and substituting $Z = \bar{M}_i B_i$, then

$$\kappa_i^2 \|W_i^{l+1}\|_2^2 \leq \kappa_i^2 \|W_i^{l+1}\|_*^2 \leq \frac{1}{2} \|W_i^{l+1} B_i\|_F^2, \quad (31)$$

where we use $\|X\|_F \leq \|X\|_2$. Denoting $\kappa = \min_i \kappa_i$, then

$$2\kappa^2 \sum_{i \in \mathcal{D}} \|W_i^{l+1}\|_2^2 \leq \sum_{i \in \mathcal{D}} \|W_i^{l+1} B_i\|_F^2 \leq \left\| \sum_{i \in \mathcal{D}} W_i^{l+1} B_i \right\|_F^2.$$

Substituting this to Eq.(21) and combining for $i \in \mathcal{D}$, there is

$$\kappa^2 \mathcal{L}_{l+1}^2(\mathcal{D}) \leq (\alpha + \beta)(5\sqrt{D} + \frac{1}{\tau} \mathcal{L}_l(\mathcal{D})) \mathcal{L}_{l+1}(\mathcal{D}). \quad (32)$$

where we apply $\max(|\mathcal{E}|, |\mathcal{F}|) \leq D$. Recalling the definition of a and b , we obtain

$$\mathcal{L}_{l+1}(\mathcal{D}) \leq a \mathcal{L}_l(\mathcal{D}) + b \leq a^{l+1} \mathcal{L}_0(\mathcal{D}) + b \frac{1 - a^{l+1}}{1 - a} \quad (33)$$

by the pre-setting $0 < a < 1$, we obtain the main theorem.

Remark 2 *Theorem 3 establishes the global convergence property of the estimation error in terms of a sum of spectral norms, and further implies that the value of $\mathcal{L}_l(\mathcal{D})$ is decaying exponentially after l stages, and the algorithm is less sensitive to the initial values.*

Sparse Neural Networks

The convolutional neural networks (CNN) are powerful models for learning visual patterns from raw images. Generally speaking, the practical networks have too many parameters to fit in mobile devices or on-chip. The pursuit of neural networks with fewer parameters draw a lot of attentions, dating back to many years ago (LeCun, Denker, and Solla 1990)(Hassibi, Stork, and others 1993). Although recent advances showed that with a trained network as a warm start, a network can be highly compressed. But their experiments are mostly done on networks with large FC layers and many redundant parameters. We will explore the potential of compressing model weights by directly introducing the sparse regularizer to the loss functions, with a small and compact network, without any warm start, purely optimizing a regularized function.

For a CNN, denoting an input features map of height h , width w , and channels c_i , as $I \in \mathbb{R}^{h \times w \times c_i}$, the convolutional kernel K is in shape size of s and with c_o output channels, then $K \in \mathbb{R}^{s \times s \times m \times c_o}$.

$$O(y, x, j) = \sigma \left[\sum_i^{c_i} \sum_u^s \sum_v^s K(u, v, i, j) I(y + u - 1, x + v - 1) \right]$$

where σ is a nonlinear function like ReLU. We use y to represent the labels, and denote K as the convolution kernels, then the objective function is written as

$$\min_K \frac{1}{N} \sum_{n=1}^N L(\mathcal{F}(I_n, K), y_n) + \sum H(K). \quad (34)$$

where L is the loss function, $\mathcal{F}(I_n, K)$ is the output of network parameterized by K , and $H(K)$ is the LCNr mentioned earlier. Although the objective is mostly non-smooth

due to the ReLU layers and max-pooling layers, we can calculate the proximal steps based on the subgradient, which is obtained by back-propagation. Since the weights across different layers are with significantly different statistics, we put separate regularizer on each layer, with independent threshold and coefficient, to induce sparsity of different degrees.

For neural networks, the data samples are much more than 3D recovery, for the multi-stage algorithm, the local optimal point can not be accessed assuredly, even with a convex regularizer. Therefore, we proposed a doubly majorization-minimization, which is practical to implement. The algorithm is based on the multi-stage, gradually calibrating the regularizer into regular ℓ_1 regularizers in each stage. While in each stage, the solver is not required to reach the local optima. The algorithm builds another (stochastic) upper bounding function $g(c, c^{l,t-1}, \mathcal{S}_t)$ for the stage-wise surrogate function $L(c) + H^l(c)$, based on the stage-wise initializer point $c^{l,0}$ and the given subset \mathcal{S}_t . For a smooth objective, $g(c, c^{l,t-1}, \mathcal{S}_t)$ can be set to be the following proximal function,

$$g(c, c^{l,t-1}, \mathcal{S}_t) = \frac{1}{|\mathcal{S}_t|} \sum_{n \in \mathcal{S}_t} [L(x_n, c^{l,t-1}) + \nabla L(x_n, c^{l,t-1})^T (c - c^{l,t-1})] + \frac{1}{2\eta} \|c - c^{l,t-1}\|^2.$$

where \mathcal{S}_t is the selected subset of dataset in the t -th step, and $1/\eta$ can be set to the smoothness parameter (if exists). Minimizing the above function can be attained by taking a proximal gradient step, $c^{l,t} \leftarrow \text{prox}_H(c^{l,t-1} - \eta \nabla L(x_n, c^{l,t-1}))$.

Algorithm 1 (Stochastic) Doubly MM Algorithms

Input $\{x_n\}_{n=1}^N$. Initialize $\lambda_i^0 = \beta$, $l = 0$, $H^0 = \beta|c|$.
repeat

Update λ_i^{l+1} as Eq.(4), and set $l = l + 1$.

repeat Solve $\min_c g(c, c^{l,t-1}, \mathcal{S}_t) + H^l(c)$ on mini-batch \mathcal{S}_k using proximal gradient descent.

until Converge

Experiments

Sparse Linear Regression

We implement a sparse linear regression model, for testing the effect of LCNr in inducing sparsity. The dataset is constructed as following, matrix $X \in \mathbb{R}^{D \times N}$ stacks $N = 1000$ random variables of $D = 256$ dimensions, drew from a Gaussian distribution, most elements of ground truth weights $\bar{w} \in \mathbb{R}^D$ are zero, the others are drew from the Gaussian distribution, the target vector $Y \in \mathbb{R}^{1 \times N}$ is obtained by $Y = \bar{w}^T X$ plus a Gaussian noise δ . The objective function is to minimize the $\frac{1}{2} \|Y - w^T X\|_F^2 + H(w)$, where we set $H(w)$ to leaky capped ℓ_1 norm, or regular ℓ_1 norm as a baseline. We use the multi-stage algorithm, which repeatedly takes gradient descent step and a proximal step. We set the maximal inner-iterations to be 20 per stage, and 50 stages in total as it converges well. We searched the regularization parameters and stepsize that perform best for problem, while

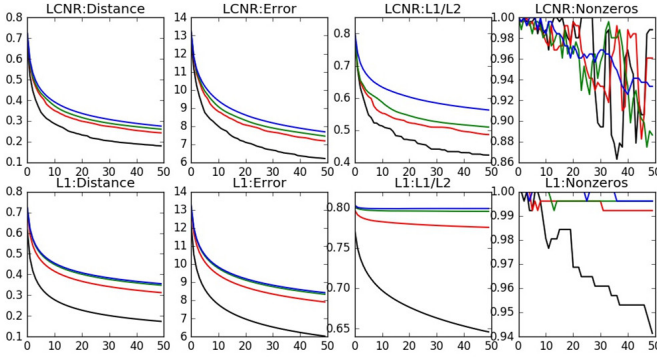


Figure 2: Performance under different measure. Black: $\beta = 100.0$, red: $\beta = 10.0$, green: $\beta = 1.0$, blue: $\beta = 0.1$. (1) the **distance** from current estimation to the ground truth as $\|w^t - \bar{w}\|_F$, (2) the **error** of linear regression as $\|Y - X^T w^t\|_F$, (3) the ratio of ℓ_1/ℓ_2 norm, as $\|w\|_1/\|w\|_2$, (4) the **nonzero** rate as $\mathbb{E}[\mathbb{I}(w_i^t \neq 0)]$.

not introducing considerable estimation bias, then, we also test several near parameters by $\times 1e - 1$. For the L1CNR, we set $\alpha/\beta = 300$.

We denote w^t as the estimated weights in t -th stage. We measure the performance by four standards. The statistic numbers change against every stage is plotted in Figure.(2). As we see from the figure, the proposed model with L1CNR converges to the ground truth with faster speed, achieving higher accuracy, and yields much sparser solutions than the ℓ_1 norm.

Human 3D Shape Recovery

We conducted the experiments to verify the effectiveness of leaky capped ℓ_1 regularization in learning sparse weights for 3D shape recovery. Our proposed algorithm is implemented in MATLAB, based on the code generously provided by (Zhou et al. 2016). We use the CMU motion capture dataset (moc) for both training and testing, thousands of frames of 3D human shapes are contained within the dataset. The shapes are annotated by 3D locations of 15 landmarks, as $S \in \mathbb{R}^{3 \times 15}$, and landmarks are at anatomical joints of human, like head, shoulders, elbows, hips, ankles and etc. The dataset contains various kinds of action. As there are large external variations across actions, we take each single action into analysis, but using the same shape dictionary. We use 300 frames of each action as test set. The rest of frames are used as training set for building shape dictionary. We set $D = 128$ to construct an over-complete dictionary by common sparse coding algorithm with ℓ_1 regularization, and the training data are pre-aligned by the Procrustes method used in (Ramakrishna, Kanade, and Sheikh 2012). The 2D shapes for test set are synthesized from the ground truth 3D shapes at different angles across 360 degrees. The recovery error is measured by the Frobenius norm $\|\hat{S} - S\|_F$ from the recovered 3D shape \hat{S} with the ground truth S . We compare our method to state-of-the-art algorithm (Zhou et al. 2016) (which has been extensively compared against other methods in their paper, like Projected Matching Pursuit (Ramakr-

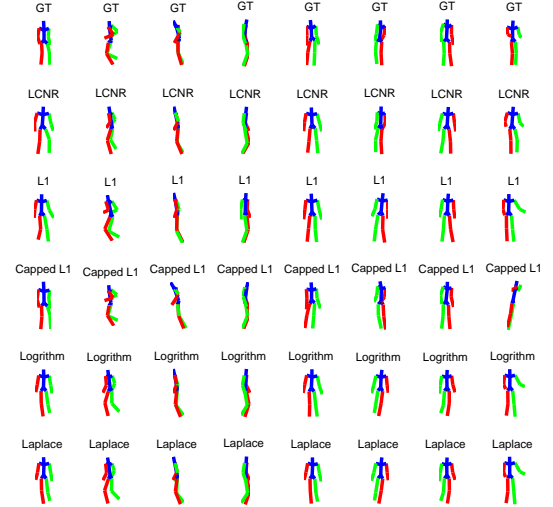


Figure 3: Recovery results of different kinds of actions, by using L1CNR and other (non)convex regularizations, and the ground truth shape (GT) on the top row.

ishna, Kanade, and Sheikh 2012) and the alternating manifold minimization method, and proved superiority, therefore we do not compare others). We conducted experiments comparing the L1CNR with other representative (non)convex regularizations, including ℓ_1 norm, capped ℓ_1 norm, logarithm norm, and Laplace norm, as

$$\text{(Convex)} \quad \ell_1 : R(c; \lambda) = \lambda |c|,$$

$$\text{capped-}\ell_1 : R(c; \lambda, \tau) = \lambda \min(|c|, \tau),$$

$$\text{logarithm} : R(c; \gamma, \lambda) = \frac{\lambda}{\log(\gamma + 1)} \log(\gamma |c| + 1),$$

$$\text{Laplace} : R(c; \lambda, \gamma) = \lambda \left(1 - \exp\left(-\frac{|c|}{\gamma}\right) \right)$$

We continue to use the doubly MM algorithm to solve the models, and the constraint on dictionary coefficients c is transferred to the spectral norm of 3D shapes $\{M_i\}$. The regularization parameters are grid searched for the best final performance. The computation complexity of calibrating τ and λ_i^l is considerably smaller than the ADMM parts, the average running time of this part is about 14% of the overall time of each iteration.

In Figure.(3), we plot the recovered shapes by L1CNR regularized and ℓ_1 regularized models, and the ground truth shapes, within a maximum inference iterations of 200. To test the performance against large noise, we also add matrix $[\sigma * \text{mean}(\text{abs}(S)) * \text{randn}(\text{size}(S))]$ to each 3D shape S before generating the 2D observation Y . Due to the limited space, we put the results in appendix. The mean errors for the testing frames of different action types decreasing against stages are shown in Figure.(4). One can see the proposed model reconstruct much more accurate skeletons than state-of-the-art model. By comparing the convergence rate in Figure (4), we see that, the non-convex regularizations generally converge faster than the ℓ_1 because they intro-

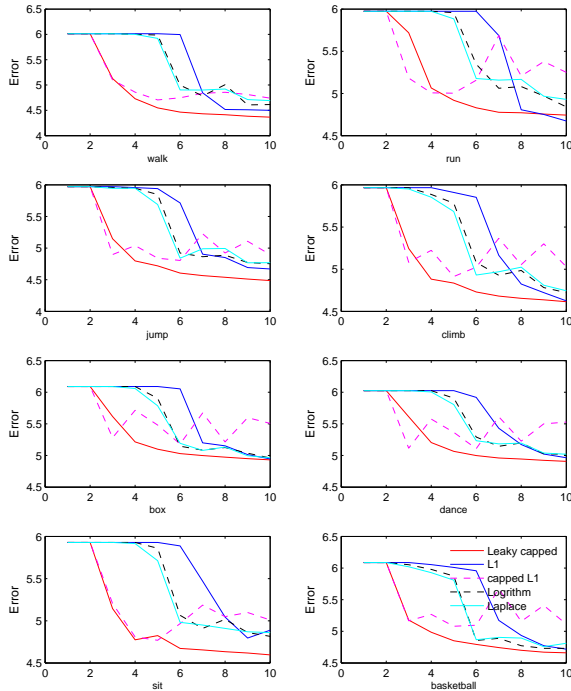


Figure 4: Convergence of recovery error with different regularizations. (X-axis: stages (for 10 inner iterations))

duce less estimation bias, so a larger coefficient λ can be adopted for acceleration. The capped norm induces faster convergence rate within the beginning 30 iterations, however, in the following iterations the estimation error oscillates up and down, indicating an unstable behavior, this indicates that a very sparse solution doesnot benefit the 3D recovery problem. The ℓ_1 regularization can achieve good estimation at last, but in the beginning the error decreases very slow, due to the imbalance between accuracy and speed, but it outperforms capped ℓ_1 , indicating that a certain degree of regularization is critical to larger weights. We can see for most of the actions, LCNR leads to higher recovery accuracy comparing opponents, achieving the same accuracy requirement within much lesser time, this improvement is significant especially to test phase, which is most the case since training phase only needs accomplished once.

Sparse Neural Networks

We implement a convolutional neural networks, with 5 convolutional layers of $5 \times 5 \times 16$ and $3 \times 3 \times 32$, three pooling layers of (2, 2), and a softmax loss layer. We use the CIFAR10 dataset. We compare the proposed LCNR with regular ℓ_1 norm regularizer. The training mini-batch size is set to be 128 per iteration, and set the maximum data passes to be 40 rounds. During each data pass, we calculate the nonzero rate of model weights, the pure loss function value without the regularizers, and test the accuracy using the testing set. For the ℓ_1 regularizer, we set parameter to be $\beta = \lambda_0$, and the parameter of LCNR is set according to $\alpha = \lambda_0 * 2.0$ and $\beta = \lambda_0 * 0.1$, therefore the penalty on larger weights are sig-

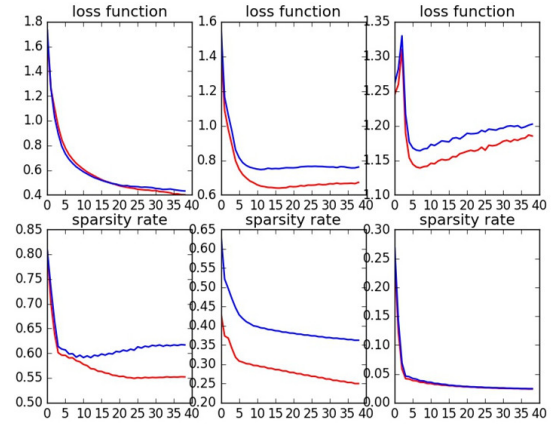


Figure 5: Statistics changing over data passes, and each column shows result of one setting. Red: LCNR regularized CNN, blue: ℓ_1 regularized CNN.

nificantly lighter than smaller ones. We grid search λ_0 within $10.0 * 2^i$ for i in range from -8 to 0 , obtaining the neural networks with different sparsity. We use the Adam solver for optimization. The initial learning rate is set to be 0.02. After each iteration, we additionally perform the proximal gradient steps $x^{l,t} = prox_{\eta R}(x^{l,t-1} - \eta \partial L(x^{l,t-1}))$, to ensure the sparsity of convolutional filters. The proximal gradient steps are like $prox_{\eta R}(x) = \text{sign}(x) \odot \max(|x| - \eta \lambda, 0)$, where \odot is the element-wise product. We plot the loss function values and sparse rates changing over time in Figure.(5) and the statistics in the final data pass in Table.(1). We jointly show the results of two methods in similar sparse rate. We can see that comparing to the ℓ_1 regularizer, the proposed LCNR achieves better sparsity, without damaging much on the loss function, and boosting the accuracy by about 2%, for achieving the same sparsity.

Table 1: Performance Statistics (each column shows result of one setting).

sparse level	method	accuracy	sparsity	loss
level-1	LCNR	70.9	55.2	0.40
	ℓ_1	68.8	61.6	0.43
level-2	LCNR	69.2	24.9	67.1
	ℓ_1	68.3	36.2	76.0
level-3	LCNR	55.8	2.3	1.18
	ℓ_1	53.2	2.4	1.20

Conclusion

In this paper, we present the leaky capped ℓ_1 norm regularizer and its multi-stage optimizer. We apply it in monocular 3D shape recovery problem, obtaining an accuracy improvement and acceleration over state-of-the-art algorithm, and prove its global convergence, the first rigorous analysis in relevant literatures and non-convex problems. Auxiliary empirical studies over sparse linear regression and convolutional neural networks show the LCNR improves upon ℓ_1 regularization.

Appendix

To test the performance against large noise, we also add matrix $[\sigma * \text{mean}(\text{abs}(S)) * \text{randn}(\text{size}(S))]$ to each 3D shape S before generating the 2D projection. Due to the limited space, we put the results in Figure 6;7;8;9.

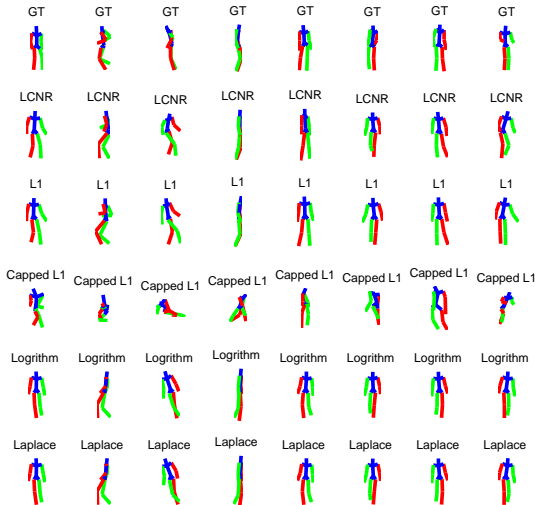


Figure 6: Recovery results of different kinds of actions, under noise condition $\sigma = 0.15$, by using LCNR and other (non)convex regularizations, and the ground truth shape (GT) on the top row.

References

- [Boyd et al. 2011] Boyd, S.; Parikh, N.; Chu, E.; Peleato, B.; and Eckstein, J. 2011. Distributed optimization and statistical learning via the alternating direction method of multipliers. *Foundations and Trends® in Machine Learning* 3(1):1–122.
- [Chen, Zhou, and Ye 2011] Chen, J.; Zhou, J.; and Ye, J. 2011. Integrating low-rank and group-sparse structures for robust multi-task learning. In *Proceedings of the 17th ACM SIGKDD international conference on Knowledge discovery and data mining*, 42–50. ACM.
- [Cootes et al. 1995] Cootes, T. F.; Taylor, C. J.; Cooper, D. H.; and Graham, J. 1995. Active shape models-their training and application. *Computer vision and image understanding* 61(1):38–59.
- [Fan and Li 2011] Fan, J., and Li, R. 2011. Variable selection via nonconcave penalized likelihood and its oracle properties. *Journal of the American Statistical Association* 96(456):1348–1360.
- [Frank et al. 1993] Frank, I. E.; Friedman, J. H.; Wold, S.; Hastie, T.; and Mallows, C. 1993. A statistical view of some chemometrics regression tools. discussion. author’s reply. *Technometrics* 35(2):109–148.
- [Friedman 2012] Friedman, J. H. 2012. Fast sparse regression and classification. *International Journal of Forecasting* 28(3):722–738.

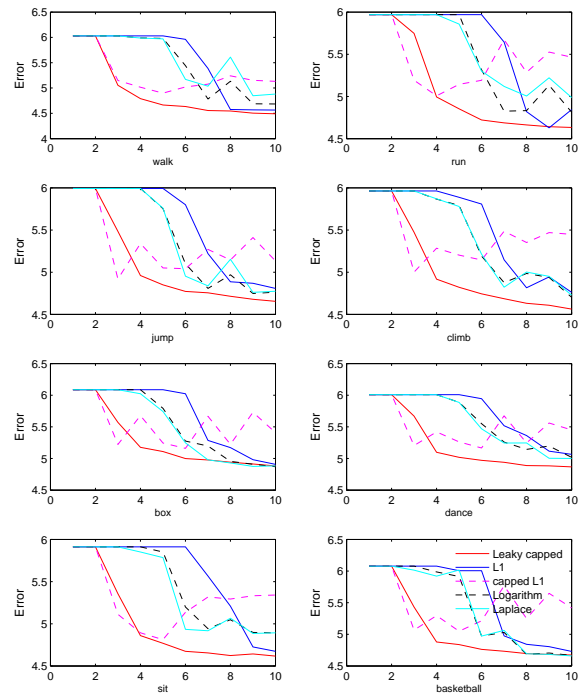


Figure 7: Convergence of recovery error under $\sigma = 0.05$ noise, with different regularizations. (X-axis: stages (for 10 inner iterations))

- [Gao et al. 2015] Gao, H.; Nie, F.; Cai, W.; and Huang, H. 2015. Robust capped norm nonnegative matrix factorization: Capped norm nmf. In *Proceedings of the 24th ACM International on Conference on Information and Knowledge Management*, 871–880. ACM.
- [Gong, Ye, and Zhang 2012] Gong, P.; Ye, J.; and Zhang, C.-s. 2012. Multi-stage multi-task feature learning. In *Advances in Neural Information Processing Systems*, 1988–1996.
- [Han and Zhang 2016] Han, L., and Zhang, Y. 2016. Multi-stage multi-task learning with reduced rank. In *AAAI*, 1638–1644.
- [Hassibi, Stork, and others 1993] Hassibi, B.; Stork, D. G.; et al. 1993. Second order derivatives for network pruning: Optimal brain surgeon. *Advances in neural information processing systems* 164–164.
- [Hejrati and Ramanan 2012] Hejrati, M., and Ramanan, D. 2012. Analyzing 3d objects in cluttered images. In *Advances in Neural Information Processing Systems*, 593–601.
- [Hunter and Lange 2004] Hunter, D. R., and Lange, K. 2004. A tutorial on mm algorithms. *The American Statistician* 58(1):30–37.
- [Jiang, Nie, and Huang 2015] Jiang, W.; Nie, F.; and Huang, H. 2015. Robust dictionary learning with capped l1-norm. In *IJCAI*, 3590–3596.
- [Journée et al. 2010] Journée, M.; Nesterov, Y.; Richtárik, P.; and Sepulchre, R. 2010. Generalized power method for

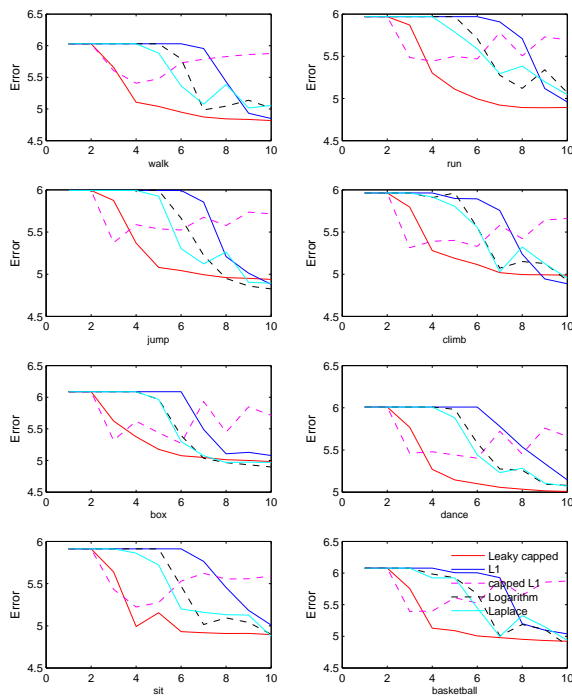


Figure 8: Convergence of recovery error under $\sigma = 0.15$ noise, with different regularizations. (X-axis: stages (for 10 inner iterations))

sparse principal component analysis. *Journal of Machine Learning Research* 11(Feb):517–553.

- [LeCun, Denker, and Solla 1990] LeCun, Y.; Denker, J. S.; and Solla, S. A. 1990. Optimal brain damage. In *Advances in neural information processing systems*, 598–605.
- [Lin et al. 2014] Lin, Y.-L.; Morariu, V. I.; Hsu, W.; and Davis, L. S. 2014. Jointly optimizing 3d model fitting and fine-grained classification. In *European Conference on Computer Vision*, 466–480. Springer.
- [Lounici et al. 2009] Lounici, K.; Pontil, M.; Tsybakov, A. B.; and De Geer, S. V. 2009. Taking advantage of sparsity in multi-task learning.
- [moc] Mocap: Carnegie mellon university motion capture database. <http://mocap.cs.cmu.edu>.
- [Parikh, Boyd, and others 2014] Parikh, N.; Boyd, S. P.; et al. 2014. Proximal algorithms. *Foundations and Trends in optimization* 1(3):127–239.
- [Ramakrishna, Kanade, and Sheikh 2012] Ramakrishna, V.; Kanade, T.; and Sheikh, Y. 2012. Reconstructing 3d human pose from 2d image landmarks. In *European Conference on Computer Vision*, 573–586. Springer.
- [Sun, Xiang, and Ye 2013] Sun, Q.; Xiang, S.; and Ye, J. 2013. Robust principal component analysis via capped norms. In *Proceedings of the 19th ACM SIGKDD international conference on Knowledge discovery and data mining*, 311–319. ACM.
- [Tang, Nie, and Jain 2016] Tang, M.; Nie, F.; and Jain, R.

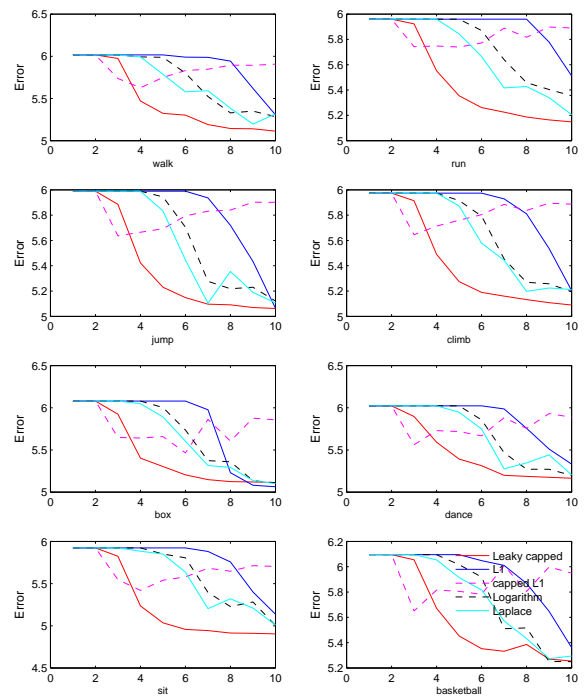


Figure 9: Convergence of recovery error under $\sigma = 0.25$ noise, with different regularizations. (X-axis: stages (for 10 inner iterations))

2016. Capped lp-norm graph embedding for photo clustering. In *Proceedings of the 2016 ACM on Multimedia Conference*, 431–435. ACM.

- [Wang et al. 2014] Wang, C.; Wang, Y.; Lin, Z.; Yuille, A. L.; and Gao, W. 2014. Robust estimation of 3d human poses from a single image. In *Proceedings of the IEEE Conference on Computer Vision and Pattern Recognition*, 2361–2368.
- [Xiang and Savarese 2012] Xiang, Y., and Savarese, S. 2012. Estimating the aspect layout of object categories. In *Computer Vision and Pattern Recognition (CVPR), 2012 IEEE Conference on*, 3410–3417. IEEE.
- [Zhang and others 2013] Zhang, T., et al. 2013. Multi-stage convex relaxation for feature selection. *Bernoulli* 19(5B):2277–2293.
- [Zhang 2010a] Zhang, C. 2010a. Nearly unbiased variable selection under minimax concave penalty. *Annals of Statistics* 38(2):894–942.
- [Zhang 2010b] Zhang, T. 2010b. Analysis of multi-stage convex relaxation for sparse regularization. *Journal of Machine Learning Research* 11(Mar):1081–1107.
- [Zhou et al. 2016] Zhou, X.; Zhu, M.; Leonardos, S.; and Daniilidis, K. 2016. Sparse representation for 3d shape estimation: a convex relaxation approach. *IEEE Transactions on Pattern Analysis and Machine Intelligence*.
- [Zia et al. 2013] Zia, M. Z.; Stark, M.; Schiele, B.; and Schindler, K. 2013. Detailed 3d representations for object recognition and modeling. *IEEE transactions on pattern analysis and machine intelligence* 35(11):2608–2623.